

Measurement of the temperature dependence of dwell time and spin relaxation probability of Rb atoms on paraffin surfaces using a beam-scattering method

Kanta Asakawa^{1,*}, Yutaro Tanaka¹, Kenta Uemura¹, Norihiro Matsuzaka²,

Kunihiro Nishikawa¹, Yuki Oguma¹, Hiroaki Usui², and Atsushi Hatakeyama^{1†}

¹*Department of Applied Physics, Tokyo University of Agriculture and Technology, Koganei, Tokyo 184-8588, Japan and*

²*Department of Organic and Polymer Materials Chemistry,*

Tokyo University of Agriculture and Technology, Koganei, Tokyo 184-8588, Japan

(Dated: August 11, 2021)

The scattering of Rb atoms on an anti-relaxation coating was studied. No significant change in the spin relaxation probability of Rb atoms by single scattering from a tetracontane surface was observed by cooling the film from 305 to 123 K. The mean surface dwell time was estimated using a time-resolved method. Delay-time spectra, from which mean surface dwell times can be estimated, were measured at 305, 153, and 123 K, with a time window of 9.3×10^{-5} s. The increase in mean surface dwell time with cooling from 305 to 123 K was smaller than 4.4×10^{-6} s, which is significantly smaller than the value expected from the mean dwell time at room temperature measured using the Larmor frequency shift. These results can be explained by assuming a small number of scattering components, with a mean surface dwell time at least three orders of magnitude longer than the majority component.

INTRODUCTION

Anti-relaxation coatings are used to reduce the spin relaxation of alkali metal atoms resulting from wall collisions in the alkali-metal vapor cells of atomic clocks [1–3] and atomic magnetometers [4–6]. Paraffin[7, 8], octadecyltrichlorosilane (OTS)[9, 10], and polydimethylsiloxane (PDMS)[11] are representative materials for anti-relaxation coatings. It has been reported that paraffin-coated surfaces can support 10^4 spin-preserving collisions for Rb atoms [8]. The performance of an anti-relaxation coating depends on the surface dwell time, as well as the strength of the interaction between alkali metal spins and the surface. The mean dwell time τ_s can be described by the Arrhenius formula:

$$\tau_s = \tau_0 \exp\left(\frac{E_{\text{des}}}{k_B T_s}\right), \quad (1)$$

where τ_0 is the pre-exponential factor, E_{des} is the desorption energy, k_B is Boltzmann constant, and T_s is the temperature of the surface. In the case of Rb atoms on tetracontane ($\text{C}_{40}\text{H}_{82}$), which is a representative type of paraffin, the experimentally obtained desorption energy is 0.06 eV[12, 13]. By adopting a commonly used assumption, i.e., that the pre-exponential factor is 1×10^{-12} s, which is the typical period of thermal vibration of atoms, we can roughly estimate τ_s as 1×10^{-11} s at 300 K. However, using the Larmor frequency shift, Ulanski *et al.* reported a mean dwell time of $(1.8 \pm 0.2) \times 10^{-6}$ s for Rb atoms on paraffin coatings at 345 K [14]. The reason for the large difference in the mean dwell time calculated from the desorption energy compared to that measured by experiments is still unclear [15]. One possibility is that the assumption $\tau_0 \simeq 1 \times 10^{-12}$ s is incorrect. By substituting $E_{\text{des}} = 0.06$ eV, $T_s = 345$ K, and $\tau_s = 1.8 \times 10^{-6}$ s into equation (1) and regarding τ_0 as

a variable, we obtain $\tau_0 = 2.4 \times 10^{-7}$ s. However, this is two orders of magnitude larger than the pre-exponential factor $\tau_0 = 2.2 \times 10^{-9}$ s of ^{87}Rb atoms on Pyrex glass surfaces coated with OTS, estimated from the temperature dependence of the mean dwell time [16] and is five orders of magnitude larger than the typical period of thermal vibration. Therefore, this issue requires further investigation.

Equation (1) shows that the mean dwell time increases with cooling, which makes it easier to measure dwell times using time-resolved methods. If we assume that $\tau_0 = 2.4 \times 10^{-7}$ s (which is obtained by substituting $E_{\text{des}} = 0.06$ eV [12, 13], $\tau_s = 1.8 \times 10^{-6}$ s, and $T_s = 345$ K [14]) is correct, then it can be seen from Eq. (1) that τ_s will increase by 6.7×10^{-5} s with cooling of a sample from 305 to 123 K, which is sufficient time to detect using time-resolved methods. The spin relaxation probability with surface scattering is also expected to increase at low temperatures due to an increased dwell time.

In this study, we investigated the temperature dependence of the spin relaxation probability and dwell time of Rb atoms on tetracontane coatings. A beam-scattering method and X-ray photoelectron spectroscopy (XPS) were employed to analyze the surface dwell time and surface chemical composition. Using an atomic beam and optical hyperfine pumping, the dwell time can be measured more directly compared to the methods used in earlier studies [14, 16]. The results show that the increase in mean dwell time (averaged over the majority of scattered atoms) with cooling from 305 to 123 K was shorter than 4.4×10^{-6} s, which is significantly shorter than the value of 6.7×10^{-5} s expected from the previously reported desorption energy $E_{\text{des}} = 0.06$ eV [12, 13] and the mean dwell time $\tau_s = 1.8 \times 10^{-6}$ s at 345 K [14]. This indicates the existence of minor scattering components with dwell times at least three orders of magnitude

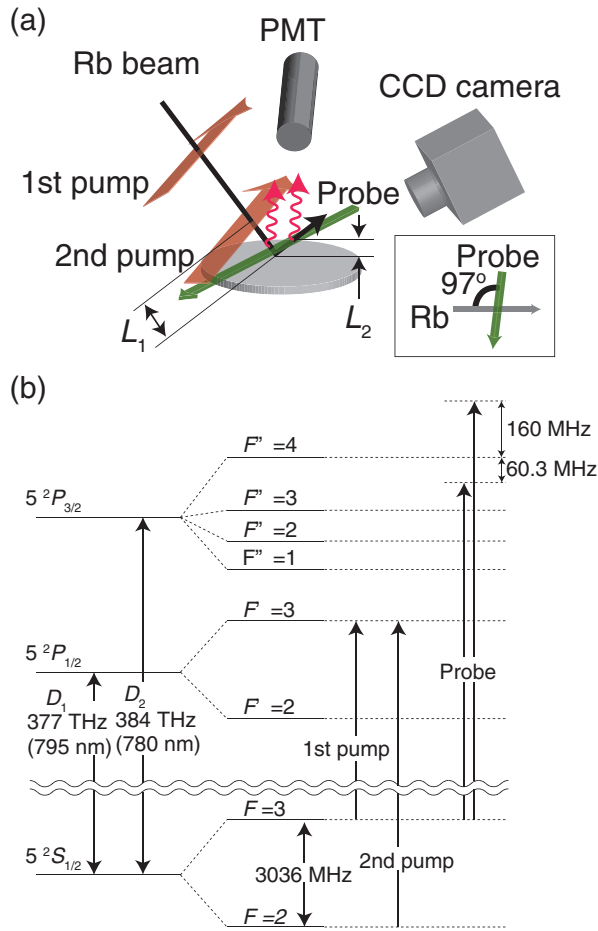


FIG. 1. (a) Schematic illustration of the experimental setup and (b) the energy-level diagram of ^{85}Rb .

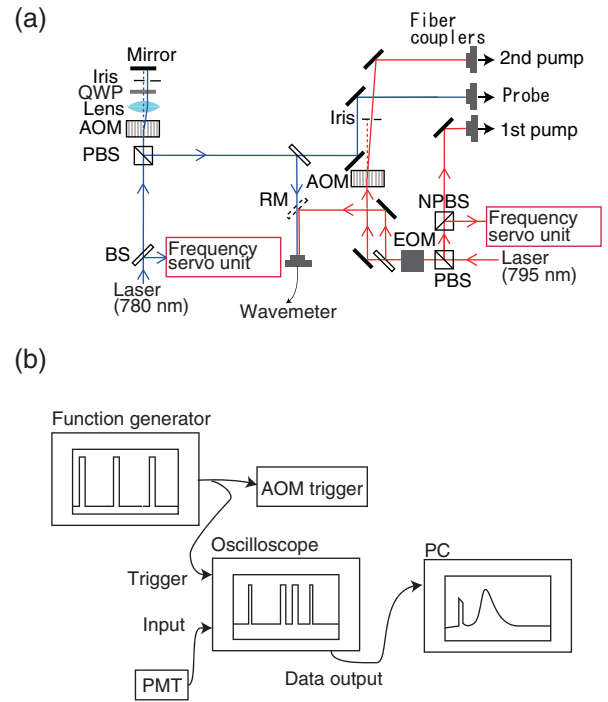


FIG. 2. (a) Schematic diagram of the optical system for generating pump and probe light. AOM, EOM, BS, PBS, NPBS, RM, and QWP denote the acousto-optic modulator, electro-optic modulator, beam splitter, polarizing beam splitter, non-polarizing beam splitter, removable mirror, and quarter-wave plate, respectively. (b) Schematic diagram of the signal-processing system used for the delay-time measurements.

larger than that of the major component.

EXPERIMENTAL

Figure 1(a) shows the experimental setup. A tetracontane-coated quartz substrate was mounted in an ultra-high vacuum (UHV) chamber with a base pressure lower than 3×10^{-7} Pa. The tetracontane film was deposited on the substrate in another high-vacuum chamber, the base pressure of which was 1.0×10^{-5} Pa, by evaporating tetracontane at 513 K for 10 min. The thickness and average roughness, R_a , of the film were measured to be 0.93 ± 0.17 μm and 50 nm, respectively, using atomic force microscopy. The Rb beam was generated using a multi-channel effusive atomic beam source. The full width at half maximum of the atomic beam at the position of the sample was estimated to be 8.2 mm from a fluorescence image taken with a charge-coupled device (CCD) camera.

The two pump light beams were directed perpendicular to the Rb beam. The pump and probe frequencies are

shown in Fig. 1(b). The optical system used to generate the pump and probe light is illustrated in Fig. 2(a). The frequency of the first pump light was tuned to the $F = 3 \rightarrow F' = 3$ transition frequency of the ^{85}Rb D_1 transition line using polarization spectroscopy [17, 18], where F and F' are the total angular momentum of atoms in the $5^2S_{1/2}$ and $5^2P_{1/2}$ states, respectively. The second pump light, the frequency of which was tuned to the $F = 2 \rightarrow F' = 3$ transition frequency of the D_1 line, was generated by blue-detuning the first pump light by 3,036 MHz [19, 20] using an electro-optic modulator (EOM) and an acousto-optic modulator (AOM), and was pulsed to 5×10^{-6} s by the AOM.

The probe light was used to selectively excite Rb atoms in the $F = 3$ state to the $F'' = 4$ state through the D_2 transition, resulting in fluorescence. Here, F'' is the total angular momentum of the atoms in the $5^2P_{3/2}$ state. The fluorescence was detected by a CCD camera and a photomultiplier tube (PMT), which were equipped with interference filters that were designed to transmit only the probe light and fluorescence. The frequency of the probe light could be tuned, which enabled selective excitation of the incident or scattered atoms. For probing scattered atoms, the probe light was blue-detuned from the $F = 3 \rightarrow F'' = 4$ transition frequency of the D_2

transition line by 160 MHz, such that it did not excite incident atoms. With this frequency, the probe light excites Rb atoms whose velocity component along the probe light is 125 ± 5 m/s; these are abundant among scattered atoms [21] but negligible among incident atoms. Here, the natural line width of the Rb D_2 transition line (6.06 MHz) [22] was used to calculate the uncertainty. When probing the incident atoms, the direction of the probe light beam was the same as that used to probe the scattered atoms; however, the frequency was red-detuned by 60.3 MHz from the $F = 3 \rightarrow F'' = 4$ transition frequency. With this frequency, the probe light excites atoms with a velocity component along the probe light of -47 ± 5 m/s. Because atoms with this velocity component are found among both incident and scattered atoms, the fluorescence intensity of the incident atoms was estimated by subtracting the contribution of scattered atoms from the measured fluorescence intensity, as discussed below.

Mean dwell-time estimates were based on time-of-flight (TOF) measurements obtained using the pump and probe light. The incident Rb atoms were first pumped to the $F = 2$ state by the first pump light and subsequently irradiated with the second pump light, which was pulsed; atoms that were irradiated with the second pump light were momentarily pumped to the $F = 3$ state. The incident atoms pumped to the $F = 3$ state by the second pump light enhanced the fluorescence induced by the probe light when they reached it. The delay time in the fluorescence enhancement induced by irradiation by the second pump light is the sum of the TOF of the Rb atoms (from the second pump light to the probe light via the film surface) and the surface dwell time. The probe-light-induced fluorescence was detected by the PMT. The signal from the PMT was processed using the system shown in Fig. 2(b). Delay-time spectra were acquired by accumulating the time intervals between the irradiation of the second probe light and the detection of fluorescence by PMT. The delay-time distribution can be treated as the distribution of the sum of the TOF and the dwell time only when the hyperfine relaxation by a single collision is negligibly small. When the hyperfine relaxation by a single collision is significant, hyperfine polarization of incident atoms is lost over the surface dwell time. In this case, a large percentage of the scattered atoms experience spin relaxation while on the surface; as such, they do not contribute to the delay-time spectra. Therefore, the probability of spin relaxation resulting from surface scattering must be estimated prior to measurement of the dwell time.

To evaluate the spin relaxation resulting from a single collision, we used the first pump light and the probe light. The first pump light polarizes incident Rb atoms in the beam to the $F = 2$ state. Given that the probe-light-induced fluorescence of the incident and scattered atoms reflects the number of atoms in the $F = 3$ state, the fluorescence intensity decreases when the first pump light

is introduced. The population fraction f_i of the $F = 2$ state of the incident atoms pumped by the first pump light can be written as

$$f_i = \frac{N_2}{N_2 + N_3} \quad (2)$$

$$= 1 - \frac{N_3}{N}, \quad (3)$$

where N_2 and N_3 are the numbers of atoms in the $F = 2$ and $F = 3$ states in the incident atoms, respectively, and $N = N_2 + N_3$. Because the fluorescence intensity is proportional to the number of atoms in the $F = 3$ state,

$$N_3 = CI_{i,p}, \quad (4)$$

where C is a constant and $I_{i,p}$ is the intensity of the fluorescence of incident atoms induced by the first pump light. $I_{i,p}$ can be obtained by

$$I_{i,p} = i_{-60.3 \text{ MHz},p} - i_{160 \text{ MHz},p} \times \frac{M(-47 \text{ m/s}, T_s)}{M(125 \text{ m/s}, T_s)} \quad (5)$$

where $i_{\delta,p}$ is the fluorescence intensity measured with the first pump light introduced with the probe light blue-detuned by δ from the $F = 3 \rightarrow F'' = 4$ transition frequency, and $M(v, T_s)$ is the Maxwell distribution given by

$$M(v, T_s) = \sqrt{\frac{2m}{\pi k_B T_s}} \exp\left(-\frac{mv^2}{2k_B T_s}\right), \quad (6)$$

where m is the mass of an ^{85}Rb atom. The first term in Eq. (5) includes contributions from both incident and scattered atoms. To subtract the latter, the second term is introduced. The second term is the fluorescence intensity of the scattered atoms excited by the probe light red-detuned by 60.3 MHz estimated from the fluorescence intensity measured with the probe light blue-detuned by 160 MHz (based on the fact that the velocity distribution of the scattered atoms can be expressed as a Maxwell distribution [21]).

Because $F = 2$ and $F = 3$ states have five- and seven-fold degeneracy, N_3 and N can be written as

$$N = \frac{12}{7} CI_{i,np}. \quad (7)$$

Here, $I_{i,np}$ is the intensity of the fluorescence of incident atoms without the first pump light, which can be obtained by

$$I_{i,np} = i_{-60.3 \text{ MHz},np} - i_{160 \text{ MHz},np} \times \frac{M(47 \text{ m/s}, T_s)}{M(125 \text{ m/s}, T_s)}, \quad (8)$$

where $i_{\delta,np}$ is the intensity of fluorescence measured with the probe light blue-detuned by δ with the first pump

219 light blocked. Therefore, we can experimentally deter-
 220 mine f_i as

$$f_i = 1 - \frac{7}{12} \frac{I_{i,p}}{I_{i,np}}. \quad (9)$$

221 Similarly, the population fraction f_s of the $F = 2$ state
 222 of the scattered atoms is written as

$$f_s = 1 - \frac{7}{12} \cdot \frac{I_{s,p}}{I_{s,np}}, \quad (10)$$

223 where $I_{s,p}$ and $I_{s,np}$ are the intensities of the fluorescence
 224 of the scattered atoms measured with the probe light
 225 blue-detuned by 160 MHz with and without the pump
 226 light, respectively. The fluorescence of the incident atoms
 227 is negligible when the probe laser is blue-detuned by 160
 228 MHz, which was confirmed by the fluorescence intensity
 229 being lower than the detection limit when the sample was
 230 removed from the atomic beam position. By comparing
 231 f_i and f_s , the proportion of atoms whose total angular
 232 momentum is changed by scattering at the surface can
 233 be estimated.

234 The delay-time and spin-relaxation measurements
 235 were conducted using different samples prepared by the
 236 same procedure, to minimize aggregation of Rb atoms,
 237 which may contaminate the surface. The aggregation of
 238 Rb on the surface resulting from atomic Rb beam irradiation
 239 was checked by XPS using Al $K\alpha$ radiation with a
 240 photon energy of 1486.6 eV.

241 RESULTS AND DISCUSSION

242 X-ray photoelectron spectroscopy

243 Aggregation of Rb atoms on the surface was investi-
 244 gated by XPS. The temperature at which aggregation
 245 was noticeable was approximately 123 K; this varied
 246 slightly among samples. Figure 3 shows the XPS spectra
 247 of the as-prepared sample and the spectra taken after ex-
 248 posing the sample to an atomic Rb beam with a flux of
 249 10^{11} – 10^{12} s^{-1} at 153 K for 2 h and 123 K for 2 h. The
 250 spectrum of the as-prepared sample displayed a strong
 251 peak at $E - E_F = -285$ eV, which was assigned to the
 252 C 1s state. After exposure to the Rb beam at low tem-
 253 perature, new peaks appeared at $E - E_F = -531$, -246 ,
 254 -238 , and -109 eV; these were assigned to the O 2p,
 255 Rb 3p_{1/2}, Rb 3p_{3/2}, and Rb 3d states, respectively. The
 256 existence of the O 2p peak indicates that some of the
 257 adsorbed Rb atoms had become oxidized by the residual
 258 O₂ or H₂O in the UHV chamber.

259 Spin relaxation resulting from surface scattering

260 The spin relaxation caused by surface scattering was
 261 evaluated at 305, 153, and 123 K. The temperature of the

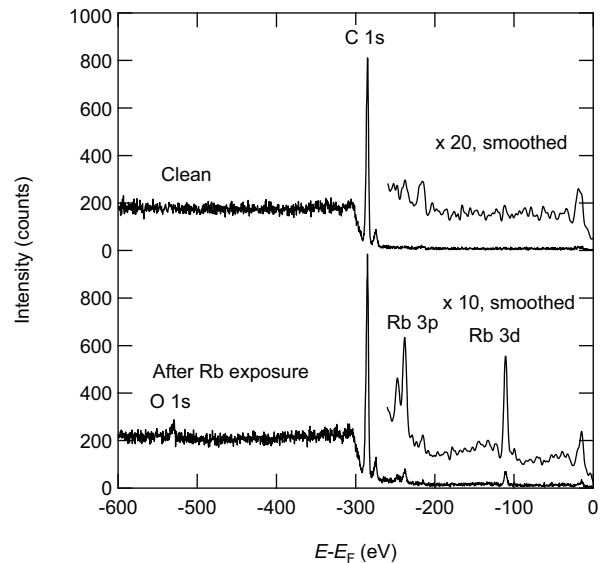


FIG. 3. X-ray photoelectron spectroscopy spectra of the clean sample and the sample exposed to an Rb beam at 153 K for 2 h and 123 K for 2 h.

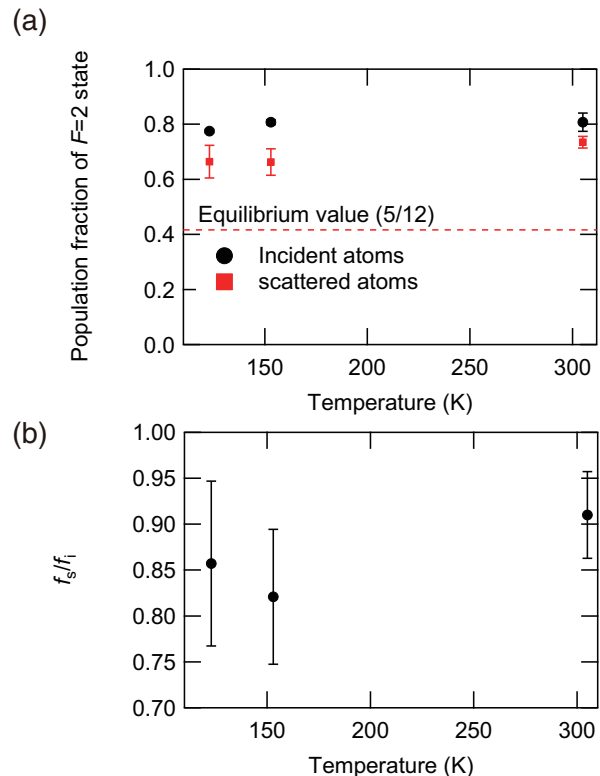


FIG. 4. (a) Temperature dependence of the $F = 2$ population fraction of the incident and scattered atoms, f_i and f_s , respectively and (b) the temperature dependence of the ratio f_s/f_i of the incident and scattered atoms.

262 Rb oven of the Rb beam source was set to 393 K. Under
 263 these conditions, the flux intensity was estimated to be
 264 $10^{11} - 10^{12}$ atoms per second based on the designed value
 265 and the fluorescence induced by the probe light. Below
 266 123 K, the number of scattered atoms was significantly
 267 smaller than at above 123 K, indicating the initiation of
 268 Rb atom adsorption at around 123 K, which is consistent
 269 with the XPS results. Figure 4(a) shows the population
 270 fractions of the $F = 2$ state for the incident and scat-
 271 tered atoms. Uncertainties in the population fractions
 272 were estimated by repeating the measurements three to
 273 five times. Because the spin relaxation induced by a sin-
 274 gle scattering process is negligibly small at room tem-
 275 perature [8], the difference between f_s and f_i at 305 K
 276 is attributed to the incident atoms away from the beam
 277 center, as opposed to relaxation due to scattering. When
 278 measuring the population fraction of the $F = 2$ state of
 279 incident atoms, atoms that pass the edge of the atomic
 280 beam are difficult to pump or detect due to the large
 281 deviation in velocity direction with respect to the major
 282 component of the incident atoms, which the pump and
 283 probe light frequencies are tuned to excite. However,
 284 when the probe light is blue-detuned to detect only the
 285 scattered atoms, atoms that were not pumped can be
 286 detected, as surface scattering changes the direction of
 287 the translational movement of atoms. The temperature
 288 dependence of the ratio of the population fraction of the
 289 incident and scattered atoms f_s/f_i is shown in Fig. 4(b);
 290 no increase in spin relaxation probability induced by cool-
 291 ing was observed above 123 K within the experimental
 292 error. Given that Rb atoms experience 10^4 collisions be-
 293 fore their spins relax [8] in paraffin-coated cells at room
 294 temperature, the low spin relaxation probability at 123
 295 K means that the mean dwell time at 123 K is smaller
 296 than 10^4 times the mean dwell time at 300 K. Thus, from
 297 Eq. (1), $\tau_0 \exp\left(\frac{E_{\text{des}}}{k_B \cdot 123 \text{ K}}\right) \leq 10^4 \cdot \tau_0 \exp\left(\frac{E_{\text{des}}}{k_B \cdot 305 \text{ K}}\right)$. By
 298 solving this, we obtain $E_{\text{des}} \leq 0.16 \text{ eV}$, which agrees with
 299 $E_{\text{des}} = 0.06 \text{ eV}$ from previous reports [12, 13].

300 Delay-time spectra

301 Figure 5(a) shows the delay-time spectrum at $T_s = 303$
 302 K. The intervals of the second pump light pulses were
 303 $2.00 \times 10^{-4} \text{ s}$. During the measurement, spectra with and
 304 without the second pump light were acquired by switch-
 305 ing the second pump light repeatedly using a shutter.
 306 The delay-time spectrum was obtained by subtracting
 307 the latter from the former. For this measurement, the
 308 temperature of the Rb oven of the beam source was set
 309 to 453 K, which was 60 K higher than that used for the
 310 low-temperature measurement, to achieve higher signal
 311 intensity. As a result, the signal intensity was enhanced
 312 by a factor of ~ 20 . The feature at $0-1.0 \times 10^{-5} \text{ s}$ is
 313 attributed to the second pump light, which partially pene-

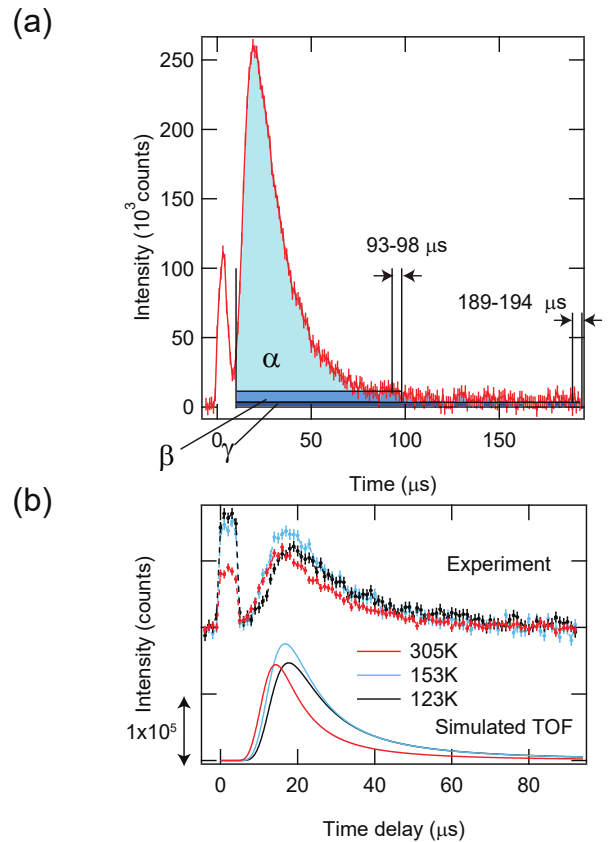


FIG. 5. Delay-time spectra (a) at 303 K taken with a high-intensity Rb beam and long repetition period (b) at 305, 153, and 123 K. Dots with error bars represent the experimental data and solid lines represent the simulation results.

314 trated the interference filter, and the fluorescence of the
 315 incident atoms; this is excluded from the intensity in-
 316 tegration discussed below. The time origin was defined
 317 by the rising edge of the second pump light-derived fea-
 318 ture. The feature peaking at around $2 \times 10^{-5} \text{ s}$ was at-
 319 tributed to the enhanced fluorescence of scattered atoms
 320 caused by the second pump light. The peak area obtained
 321 by integrating the intensity in the region 1.0×10^{-5} –
 322 $1.89 \times 10^{-4} \text{ s}$ and subtracting the average level of the
 323 region 1.89×10^{-4} – $1.94 \times 10^{-4} \text{ s}$ as the base level, which
 corresponds to the sum of the area of the regions repre-
 sented by α and β in Fig. 5 (a), accounted for $91 \pm 5\%$
 of the total signal intensity. Here, the total signal intensity
 is the sum of regions α , β , and γ . If we adopt the average
 level of the region 9.3×10^{-5} – $9.8 \times 10^{-5} \text{ s}$ as the base
 level, the integrated intensity in the region 1.0×10^{-5} –
 $9.3 \times 10^{-5} \text{ s}$, which corresponds to the area of region α ,
 accounts for $79 \pm 2\%$ of the total intensity. This implies
 that $79 \pm 2\%$ of the scattered atoms will contribute to
 the peak intensity in the delay-time spectra, if we regard
 the sum of the region $t < 9.3 \times 10^{-5} \text{ s}$ as the peak in-
 tensity and adopt the average level of the region 9.3×10^{-5} –
 $9.8 \times 10^{-5} \text{ s}$ as the base level. For the temperature-

dependence measurement, we used 1.00×10^{-4} s as the second pump light interval and subtracted the average of the region near the back edge of the time window from the whole spectra, instead of subtracting the background spectra taken without the second pump light. This dramatically reduced the measurement time, which was essential to prevent Rb aggregation during measurements at low temperatures.

Figure 5 (b) shows the delay-time spectra taken at 305, 153, and 123 K. The temperature of the Rb oven of the Rb beam source was set to 393 K. By cooling the tetracontane film from 305 to 123 K, the delay-time spectrum shifted to the longer side and the mean delay time τ_M increased by $(7.0 \pm 3.2) \times 10^{-6}$ s from $(2.54 \pm 0.21) \times 10^{-5}$ to $(3.24 \pm 0.24) \times 10^{-5}$ s. Here, τ_M is defined by

$$\tau_M = \frac{\sum_i t_i I_i}{\sum_i I_i}, \quad (11)$$

where t_i and I_i are the delay time and the intensity at the i th point, respectively. The uncertainty in τ_M originates from the uncertainty in I_i at each point, which is $\sqrt{I_i}$. Data points in the region $6 \times 10^{-6} \leq t_i < 9.3 \times 10^{-5}$ s were included in the summation. The average of the region $9.5 \times 10^{-5} \text{ s} \leq t_i < 9.9 \times 10^{-5} \text{ s}$ was adopted as the base level. Intensities between 0 and 6×10^{-6} s, which include the peak originating from the second pump light, were not included in the summation. Because the velocity distribution of the scattered beam also depends on the film temperature [21], we cannot simply attribute the increase in τ_M to the increase in mean dwell time. To evaluate the increase in TOF due to the change in velocity distribution, we simulated TOF spectra without taking the dwell time into account.

The simulation considered the TOF from the second pump light to the surface, and from the surface to the probe light. The velocity distribution $d_b(v)$ of the incident atoms, and the TOF distribution from the second pump light to the surface $D_b(t, L_1)$, were calculated using equations [21]

$$d_b(v) = \frac{m^2}{2k_B^2 T_b^2} v^3 \exp\left(-\frac{mv^2}{2k_B T_b}\right), \quad (12)$$

$$D_b(t, L_1) = d_b\left(\frac{L_1}{t}\right) \frac{d}{dt} \left(\frac{L_1}{t}\right) = \frac{m^2 L_1^4}{2k_B^2 T_b^2 t^5} \exp\left(-\frac{m}{2k_B T_b} \left(\frac{L_1}{t}\right)^2\right), \quad (13)$$

where T_b is the temperature of the incident beam determined by the temperature of the capillary of the beam source, v is the velocity of atoms, L_1 is the distance between the second pump light and the surface along the atomic beam direction, and t is the time. T_b was 453 K, and L_1 was roughly estimated to be 1.8×10^{-3} m. The distribution $d_s(v_{\perp s})$ of the velocity component of the scattered atoms perpendicular to the surface, which

are in thermal equilibrium with the film, and the TOF distribution $D_s(t, L_2)$ are given by

$$d_s(v_{\perp s}) = \sqrt{\frac{2m}{\pi k_B T_s}} \exp\left(-\frac{mv_{\perp s}^2}{2k_B T_s}\right), \quad (15)$$

$$D_s(t, L_2) = d_s\left(\frac{L_2}{t}\right) \frac{d}{dt} \left(\frac{L_2}{t}\right) \quad (16)$$

$$= \sqrt{\frac{2m}{\pi k_B T_s}} \frac{L_2}{t^2} \exp\left(-\frac{m}{2k_B T_s} \left(\frac{L_2}{t}\right)^2\right) \quad (17)$$

where $v_{\perp s}$ is the velocity component perpendicular to the film surface, and L_2 , which was estimated to be 1.42×10^{-3} m, is the height of the probe light from the film surface [21]. The total TOF spectrum $S(t)$ is given by

$$S(t) = \frac{1}{w} \int_{t-w}^t dr \int_0^r ds u_b(s, L_1) \times u_s(r-s, L_2), \quad (18)$$

where

$$u_b(t, L_1) = \int_0^\infty \frac{1}{\sqrt{2\pi\sigma_1^2}} \exp\left(-\frac{(x-L_1)^2}{2\sigma_1^2}\right) \times D_b(t, x) dx, \quad (19)$$

$$u_s(t, L_2) = \int_0^\infty \frac{1}{\sqrt{2\pi\sigma_2^2}} \exp\left(-\frac{(x-L_2)^2}{2\sigma_2^2}\right) \times g_s(t, x) dx, \quad (20)$$

where w is the duration of the second pump light and σ_1 and σ_2 are the $1/\sqrt{e}$ half width of the second pump light and probe light, respectively. σ_1 and σ_2 were 2.4×10^{-4} and 1.7×10^{-4} m, respectively.

The simulation results are indicated by solid lines in Fig. 5. The intensities of the simulation results were adjusted to fit the experimental results. The simulated TOF spectra are in good agreement with the experimental results. According to the simulation results at 305 K, the peak area calculated by integrating the spectral intensity between 1.0×10^{-5} and 9.3×10^{-5} s and subtracting the average of the region 9.3×10^{-5} – 9.8×10^{-5} s accounts for 81% of the total intensity, which is in good agreement with the experimental results shown in Fig. 5(a). The simulated mean TOF calculated from the region 0– 9.3×10^{-5} s increased by 5.8×10^{-6} s from 2.48×10^{-5} to 3.06×10^{-5} s with cooling from 305 to 123 K. Here, the average of the region $9.5 \times 10^{-5} \text{ s} \leq t_i < 9.9 \times 10^{-5} \text{ s}$ was adopted as the base level. The experimentally observed shift of τ_M , which is $(7.0 \pm 3.2) \times 10^{-6}$ s, is the sum of the increase in mean dwell time and mean TOF. Therefore, the increase in mean dwell time induced by cooling can be obtained by subtracting the increase in the simulated mean TOF from the experimentally obtained increase in the mean delay time. Therefore, we can see from the experimental and simulation results that

$$\tau_{s,t < 93 \mu\text{s}}(123 \text{ K}) - \tau_{s,t < 93 \mu\text{s}}(305 \text{ K}) = (1.2 \pm 3.2) \times 10^{-6} \text{ s}, \quad (21)$$

414 which means

$$\tau_{s,t < 93 \text{ } \mu\text{s}}(123 \text{ K}) - \tau_{s,t < 93 \text{ } \mu\text{s}}(305 \text{ K}) \leq 4.4 \times 10^{-6} \text{ s.} \quad (22)$$

415 Here, $\tau_{s,t < t_{\max}}(T_s)$ is the mean dwell time of the scatter-
416 ing component, with a delay time of less than t_{\max} at a
417 surface temperature of T_s .

418 Discussion

419 The discrepancy between our result ($\tau_s(123 \text{ K}) -$
420 $\tau_s(305 \text{ K}) \leq 4.4 \times 10^{-6} \text{ s}$) and the value ($\tau_s(123 \text{ K}) -$
421 $\tau_s(305 \text{ K}) = 6.7 \times 10^{-5} \text{ s}$) obtained by substituting the
422 desorption energy $E_{\text{des}} = 0.06 \text{ eV}$ [12, 13] and mean
423 dwell time $\tau_s = 1.8 \times 10^{-6} \text{ s}$ at $T = 345 \text{ K}$ [14] into
424 Eq. (1) may be explained by assuming multiple scatter-
425 ing components with different mean dwell times. Using
426 the method described in this study, the scattering com-
427 ponents with dwell times larger than $9.3 \times 10^{-5} \text{ s}$ is not
428 detected. In Ref. [14], on the other hand, the mean dwell
429 time was estimated based on the Larmor frequency shift
430 caused by the interaction with the surface and evanescent
431 pump light.

432 The reason for the difference in mean dwell times be-
433 tween the scattering components can be attributed to
434 differences in pre-exponential factors. It has been re-
435 ported that a certain proportion of the incident atoms
436 penetrate the PDMS film, diffuse into the bulk, and des-
437 orb from the surface [15], which makes the mean dwell
438 time about a million times larger than that calculated
439 from the desorption energy and film temperature. If the
440 diffusion barrier in the bulk is significantly smaller than
441 the desorption energy, the temperature dependence of the
442 diffusion time can be neglected so that the temperature
443 dependence of the mean dwell time is almost entirely de-
444 termined by the desorption energy. By assuming that two
445 scattering components with different mean dwell times
446 exist, we can approximate the temperature dependence
447 of the mean dwell time as

$$\tau_s = (1 - p)\tau_1 \exp\left(\frac{E_{\text{des}}}{k_B T_s}\right) + p\tau_2 \exp\left(\frac{E_{\text{des}}}{k_B T_s}\right), \quad (23)$$

448 where p is the proportion of scattering events with
449 longer mean dwell times, and τ_1 and τ_2 are the pre-
450 exponential factors for the scattering events with shorter
451 and longer mean dwell times, respectively. We sup-
452 pose that $\tau_2 \exp\left(\frac{E_{\text{des}}}{k_B T_s}\right)$ is significantly larger than the
453 time window of $9.3 \times 10^{-5} \text{ s}$ and only the component
454 with a shorter mean dwell time, which corresponds to
455 the first term in Eq. (23), contributes to the delay-
456 time spectra. By substituting Eq. (1) into our re-
457 sults ($\tau_s(123 \text{ K}) - \tau_s(305 \text{ K}) \leq 4.4 \times 10^{-6} \text{ s}$), we obtain
458 $0 < \tau_1 \leq 1.6 \times 10^{-8} \text{ s}$. From $\tau_2 \exp\left(\frac{E_{\text{des}}}{k_B T_s}\right) \gg 9.3 \times 10^{-5}$

459 s at $T_s \leq 305 \text{ K}$, we get $\tau_2 \gg 9.47 \times 10^{-6} \text{ s}$. By substi-
460 tuting $\tau_s = 1.8 \times 10^{-6} \text{ s}$ at 345 K [14] and $E_{\text{des}} = 0.06$
461 eV [12, 13] into Eq. (23), $p = \frac{2.4 \times 10^{-7} \tau_s - \tau_1}{\tau_2 - \tau_1}$. From $0 < \tau_1$
462 and $\tau_2 \gg 9.47 \times 10^{-6} \text{ s}$, $p < 0.025$, which means that the
463 component with a shorter mean dwell time is the major
464 component. This is consistent with the fact that the ob-
465 served $79 \pm 2 \%$ fraction within $9.3 \times 10^{-5} \text{ s}$ is nearly the
466 same as the 81% fraction obtained from the simulation
467 without dwell times.

CONCLUSIONS

Scattering of Rb atoms on tetracontane surfaces was investigated. No significant spin relaxation was observed with a single scattering process down to 123 K. The temperature evolution of delay time showed that the increase in mean surface dwell time induced by cooling from 305 to 123 K was less than $4.4 \times 10^{-6} \text{ s}$. Taken together, the results indicate the existence of multiple scattering sites. The pre-exponential factor τ_0 of the minor components is at least three orders of magnitude larger than that of the major component, which means that the mean dwell time of the minor scattering components is at least three orders of magnitude larger than that of the major component.

ACKNOWLEDGMENTS

This work was supported by JSPS KAKENHI Grant Number JP17H02933.

* asakawa@go.tuat.ac.jp

† hatakeya@cc.tuat.ac.jp

- [1] A. Risley, S. Jarvis Jr, and J. Vanier, *Journal of Applied Physics* **51**, 4571 (1980).
- [2] H. Robinson and C. Johnson, *Applied Physics Letters* **40**, 771 (1982).
- [3] R. Frueholz, C. Volk, and J. Camparo, *Journal of Applied Physics* **54**, 5613 (1983).
- [4] D. Budker, V. Yashchuk, and M. Zolotarev, *Physical Review Letters* **81**, 5788 (1998).
- [5] M. Balabas, D. Budker, J. Kitching, P. Schwindt, and J. Stalnaker, *Journal of the Optical Society of America B* **23**, 1001 (2006).
- [6] W. Wasilewski, K. Jensen, H. Krauter, J. J. Renema, M. Balabas, and E. S. Polzik, *Physical Review Letters* **104**, 133601 (2010).
- [7] H. Robinson, E. Ensberg, and H. Dehmelt, *Bulletin of the American Physical Society* **3** (1958).
- [8] M. A. Bouchiat and J. Brossel, *Physical Review* **147**, 41 (1966).
- [9] S. Seltzer, P. Meares, and M. Romalis, *Physical Review A* **75**, 051407 (2007).

- 507 [10] K. Zhao, M. Schaden, and Z. Wu, Physical Review A 521
508 **78**, 034901 (2008). 522
- 509 [11] S. Atutov, F. Benimetskiy, A. Plekhanov, and 523
510 V. Sorokin, The European Physical Journal D **70**, 1524
511 (2016). 525
- 512 [12] C. Rahman and H. Robinson, IEEE journal of quantum 526
513 electronics **23**, 452 (1987). 527
- 514 [13] D. Budker, L. Hollberg, D. F. Kimball, J. Kitching, 528
515 S. Pustelny, and V. V. Yashchuk, Physical Review A 529
516 **71**, 012903 (2005). 530
- 517 [14] E. Ulanski and Z. Wu, Applied Physics Letters **98**, 531
518 201115 (2011). 532
- 519 [15] S. Atutov and A. Plekhanov, Journal of Experimental 533
520 and Theoretical Physics **120**, 1 (2015). 534
- [16] K. Zhao, M. Schaden, and Z. Wu, Physical Review Let-
ters **103**, 073201 (2009).
- [17] C. Wieman and T. W. Hänsch, Physical Review Letters
36, 1170 (1976).
- [18] M. Harris, C. Adams, S. Cornish, I. McLeod, E. Tarleton,
and I. Hughes, Physical Review A **73**, 062509 (2006).
- [19] E. Arimondo, M. Inguscio, and P. Violino, Reviews of
Modern Physics **49**, 31 (1977).
- [20] B. Schultz, H. Ming, G. Noble, and W. Van Wijngaard-
den, The European Physical Journal D **48**, 171 (2008).
- [21] N. Sekiguchi, A. Hatakeyama, K. Okuma, and H. Usui,
Physical Review A **98**, 042709 (2018).
- [22] U. Volz and H. Schmoranzer, Physica Scripta **1996**, 48
(1996).